Proceedings of the 30th Conference
on Decision and Control
Brighton, England • December 1991

Design and Control of a Two-Degree-of-Freedom Lightweight Flexible Arm

Vincente Feliu
Dpto Ingenieria Electrica, Electronica y Control
E.T.S.I. Industriales UNED
Madrid, Spain.

Kuldip S. Rattan
Department of Electrical Engineering
Wright State University
Dayton, OH 45435, USA.

H. Benjamin Brown Jr.
Robotics Institute
Carneigie Mellon University
Pittsburgh, PA 15213, USA.

Abstract

This paper describes the design and control of an efficient two-joint, two-links flexible arm. This efficient arm was designed and built to use most of the energy (provided by the motors) in performing the tasks instead of moving the arm structure. The arm has most of its mass concentrated at the tip and uses a special mechanical configuration to decouple radial tip motions from angular tip motions. An important problem when controlling lightweight flexible arms is the large Coulomb friction of the motors. A two-nested-loop multivariable controller is used to control the lightweight flexible arm with friction in the joints. The inner loop controls the position of the motors while the outer loop controls the tip position. The resolved acceleration method is generalized to control this flexible arm. The compliance matrix is used to model the oscillations of the structure and is included in the decoupling/linearizing term of this controller. Experimental results are presented.

1 Introduction

This paper describes the design and control of a small two-joints, two-links flexible arm that we have built in our laboratory. This arm operates in a plane on an air table. The arm is designed with exaggerated flexibility to study the control of flexible structures and is very light in weight compared to the mass placed at the tip (no mass placed at the elbow joint). The objective of this research is to design efficient and faster arms in the sense that most of the energy provided by the motors is spent in doing the task (moving the tip mass) and very little energy is wasted in moving the arm structure (unlike rigid arms).

To decouple the tip's radial motions from its angular motions, a special four-bar linkage is used to drive the elbow joint from a motor mounted near the base. The mechanics of the arm are described in Section 2. A dynamic model of this arm that can be easily extended to any n-degrees-of-freedom lumped-mass flexible arm is developed in this section.

An important problem when controlling lightweight flexible arms is the large Coulomb friction of the motors. A two-nested-loop control scheme is used to control the arm. The inner loop controls the position of the motors while the outer loop controls the tip position. The method, which is the generalization of the control method described in [1-3], is robust to changes in the dynamic friction and insensitive to Coulomb friction. A generalization of the resolved acceleration method [4] to the case of flexible arms is implemented in the outer loop. The compliance matrix is used to model the oscillations of the structure and is included in the decoupling/linearizing term of this controller. Section 3 describes the control scheme of the arm. Experimental results are given in Section 4 and conclusions are drawn in Section 5.

2 Mechanical Issues

The flexible arm was designed to fulfill two mechanical specifications:

1. The arm is very light in weight.
2. Radial motions of the tip are nearly decoupled from angular motions (if we neglect the vibrations because of flexibility).

In order to fulfill the first specification, the links were made of a very lightweight wire (consequently having a significant elasticity) and the motor which moves the elbow was placed close to the base of the arm. A four-bar linkage was used to transmit the motion of the motor to the elbow. To fulfill the second specification, the length of the two links was made identical and the dimensions of the four-bar linkage were specifically designed.

Subsections 2.1. and 2.2. study the kinematics and dynamics of the arm under the assumption that it is rigid. Subsection 2.3. discusses the flexibility effects.

2.1 Kinematics

Figure 1 illustrates the kinematics of the arm, neglecting its compliance. The arm is composed of a four-bar linkage with pivots at points O, A, B and C, and at the tip position P. Note that the length of link O-A is twice that of link B-C and the links O-C and C-P are of equal length. With points O and A fixed (for the sake of studying kinematic behavior, otherwise, A is normally not fixed), it can be shown that the tip describes a path very close to a straight line through the origin (O) at an angle of 45 degrees to the X-axis. That is, as the radius to the tip (ρ) varies, the tip angle (γ) remains close to 45 degrees (γ_0). The point P_0 is the ideal tip position assuming that

$$\rho = \rho_0 = 2l\cos(\varphi - 45^\circ). \qquad (1)$$

Figure 2 shows the normalized errors in the tip position as a function of the normalized tip radius ($\rho/(2l)$) for several values of parameter α (a/l). The value $\rho/(2l)$ represents the percentage of arm extension and has a maximum range of 0 - 1.0. For a typical value of α, say 0.2, we see from the plot that the deviations are quite small ($< 1\%$) in the range of $0.4 < \rho/(2l) < 0.8$ and less than 5 % in the range $0.25 < \rho/(2l) < 0.9$. Thus, by restricting the range of motion of the arm, we can minimize the deviation from ideal behavior. This deviation requires consideration for precise tip positioning, however, in the kinematic calculations, the effects can be ignored with regard to system dynamics. This can simplify dynamic calculations substantially.

This kinematic design provides a means of decoupling the two joint actuators. We mount one of the actuators so that it drives link O-A with respect to ground. The net effect is a tangential force at the tip. We mount the second actuator so that it drives link O-C with respect to link O-A. Thus, it generates equal and opposite torques on the two links and the net effect is a radial force at the tip. In terms of position control, a displacement of the first actuator generates a pure tangential motion while the displacement of the second actuator produces a pure radial motion. The decoupling effects are based on the ideal (straight-line) behavior of the arm, however, there will be some deviation from this fully decoupled behavior, especially near the extremes of travel

($\rho = 0$, $\rho = 1$) of the arm. One consequence of this geometry is that there is approximately zero coupling between the actuators, i.e., a torque at one actuator generates very little reaction torque at the other. This simplifies control and possibly reduces energy usage of the arm.

2.2 Rigid arm dynamics

In this subsection, the dynamics of the arm is developed assuming that it is rigid. The links are assumed to be approximately massless. A complete model that contains effects of the link compliance is developed in the next subsection. Using Lagrange equations (or Newton-Euler equations), we get

$$\begin{pmatrix} F_\rho \\ F_\gamma \end{pmatrix} = m\left(\begin{pmatrix} \ddot{\rho} \\ \rho\ddot{\gamma} \end{pmatrix} + \begin{pmatrix} -\rho\dot{\gamma}^2 \\ 2\dot{\rho}\dot{\gamma} \end{pmatrix}\right). \tag{2}$$

where F_ρ, F_γ are the radial and angular forces applied to the tip, respectively, (ρ, γ) are the polar coordinates of the tip and m is the tip mass. Because of the decoupling between the two motors and by applying the principle of virtual work, the torques T_1 and T_2 generated by the motors can be written as

$$\begin{pmatrix} T_1 \\ T_2 \end{pmatrix} \approx \begin{pmatrix} 0 & 2l\cos(\varphi) \\ 2l\sin(\varphi) & 0 \end{pmatrix} \begin{pmatrix} F_\rho \\ F_\gamma \end{pmatrix}. \tag{3}$$

2.3 Compliance

For a system (4-joint, planar arm) that can be modelled as having all of its mass concentrated at the tip, it is useful to think in terms of the compliance at the tip. Control of the tip mass then becomes a matter of producing deflections to generate the appropriate tip forces. This is the two-dimensional equivalent of deflecting a spring to generate a force.

It can be shown that the compliance (or stiffness) of a linear, two-dimensional system can be defined by two, orthogonal stiffness values [5]. The general relationship between forces and displacements is given by

$$\begin{pmatrix} F_x \\ F_y \end{pmatrix} = \begin{pmatrix} k_{1,1} & k_{1,2} \\ k_{2,1} & k_{2,2} \end{pmatrix} \begin{pmatrix} \delta x \\ \delta y \end{pmatrix} \tag{4}$$

where F_x and F_y are forces applied to tip; δx and δy are tip deflections; and $k_{i,j}$ are stiffness coefficients. The question now arises as to how to find the relationship between forces and displacements, i.e., the stiffness matrix at the tip. For simple systems, these values can be calculated. For more complex systems or for confirming analytical results, we can deduce these from observations of the natural frequencies of the mechanical system. The stiffness matrix will, of course, vary with the configuration of the arm, in particular, with the extension (ρ) of the arm. Note that we have defined the stiffness matrix with respect to coordinates $X - Y$ aligned with the base-to-tip vector. We do this so that the stiffness matrix depends only on the variable ρ. Thus, a coordinate rotation is needed to transform to world coordinates. For use on a digital computer, tabular storage of stiffness parameters is indicated.

The first approach involves calculating stiffness parameters for individual links and then combining these through appropriate force/moment analysis. The stiffness parameters can be defined either in terms of principal stiffness vectors (magnitude and orientation of the principal stiffnesses) or in terms of the stiffness matrix. In either case, three values are required (for any value of the extension, ρ) and these values will be referenced to the coordinate axis aligned with the base-to-tip radius vector. Performing the analysis for our particular arm with its four-bar linkage, we get the following compliance matrix C, which is the inverse of the stiffness matrix described in expression (4)

$$\begin{pmatrix} \delta x \\ \delta y \end{pmatrix} = \begin{pmatrix} c_{1,1} & c_{1,2} \\ c_{2,1} & c_{2,2} \end{pmatrix} \begin{pmatrix} F_x \\ F_y \end{pmatrix}, \tag{5}$$

where

$$c_{1,1} = \frac{l^2\sin^2(\varphi)}{k_c}\left(1 + 4\frac{k_c}{k_b}\right) \tag{6}$$

$$c_{1,2} = c_{2,1} = l^2\sin(\varphi)\cos(\varphi)/k_c \tag{7}$$

$$c_{2,2} = l^2\cos^2(\varphi)/k_c, \tag{8}$$

and k_b, k_c are the individual stiffnesses of links O-C and C-P respectively. Notice that the stiffness of link A-B does not appear because this link is not subjected to bending, only tension and compression. Figure 3 shows the calculated stiffness vectors for various configurations of the experimental arm. While it may be more convenient for control purposes to store values of the stiffness matrix, the vector plots give a readily understandable picture of the stiffness characteristics. Double arrowheads in Figure 3 indicate vectors extend beyond available space.

The dynamic model of a two-degrees-of-freedom lightweight flexible arm with the mass concentrated at the tip can be represented by the scheme of Figure 4 using the stiffness/compliance matrix. This is a generalization of the dynamics of the rigid arm case (rigid arm dynamics are a block in this diagram). In this figure, $\hat{J}$ is the jacobian of the rigid arm kinematics that relates motor velocities to tip velocities (in our particular arm, in polar coordinates), T_F is the matrix of expression (3) that transforms tip forces into motor torques, F is the tip force, P is the tip position and Θ_{me} are the corresponding joint coordinates (actuator coordinates) assuming that the arm is undeflected.

3 Control issues

3.1 General scheme

Our arm presents two special problems that most other arms do not have: a large Coulomb friction in the joints and flexibility in the links. This requires the design of a special controller which is described in this section. We use four measurements to control this arm: a tracking camera gives the tip position in cartesian coordinates (x, y) and two potentiometers mounted on the motors to give the motor position (joint angles). Because the arm has been designed in such a way that its rigid dynamics are nearly decoupled in polar coordinates, we will use these coordinates for the tip position control. Transformation to polar coordinates from cartesian measurements given by the camera is straightforward and does not introduce any error because it does not use any kinematic parameter of the arm.

In order to remove the effects of joint Coulomb friction and of time-varying dynamic friction, a two nested multivariable loop control structure is proposed. An inner loop is closed around the motor to control the joint (motor) angles and then an outer loop is closed that controls the tip position. The general scheme of this control structure is shown in Figure 5. The inner controller uses the errors between the actual (Θ_m) and the commanded motor positions (Θ_{mr}) and generates control signals which are the currents for the two motors. The outer loop basically uses the errors between the actual (P) and the desired (P_r) positions and generates control signals which are the command positions for the motors of the inner loop. This scheme is the generalization of a control scheme that is robust to friction [1-3].

As a result of the procedure for controlling the motor position developed in the next subsection, we can describe the dynamics of the two closed-loop motors as two decoupled time invariant linear systems. If we use high enough gains in the controllers of these loops, the dynamics of these systems can be made much faster than the dynamics of the arm and, therefore, can be neglected in the design of the tip position control loop. This greatly simplifies the design method.

3.2 Motor position control loops

The control scheme described in [1-3] is used for the control of motor position. Let the dynamics of each motor be described by

$$K_i i_i = J_i \frac{d^2\theta_{mi}}{dt^2} + V_i \frac{d\theta_{mi}}{dt} + CF_i + Ct_i, \quad (9)$$

where K_i is the electromechanical constant of the motor i, i_i is its current, J_i is its polar moment of inertia, V_i is its dynamic friction coefficient, Ct_i is the coupling torque between the ith motor and the mechanical structure, CF_i is its Coulomb friction, and the subindex $i = 1, 2$, designates the motor. To compensate for Coulomb friction and the coupling torque, two feedforward terms were added to the current, $\hat{i}_i$, generated by the motor position controller,

$$i_i = \hat{i}_i + (CF_i + Ct_i)/K_i. \quad (10)$$

The first term linearizes the motor system by compensating for Coulomb friction (which is nonlinear) and the second term decouples the dynamics of the motor from the rest of the arm. We assume that Coulomb friction is of the form

$$CF_i(t) = \pm \mid CF_i \mid \quad (11)$$

where the sign is that of the motor velocity. The Coulomb friction compensation term is generated by knowing the amplitude of the Coulomb friction and by estimating the actual velocity of the motor from position measurements.

To generate the decoupling term, the coupling torque Ct may be obtained directly from the measurements of the strain gauges placed at the joints or can be estimated from the actual deflection of the arm obtained from the measurements of the motor and the tip position.

It was shown in [1-2] that closing the motor position loop with high gain controllers makes the system less sensitive to perturbations (caused by an imperfect compensation of the Coulomb friction) and to time varying parameters (dynamic friction coefficient). A discrete P.D. controller of high gains was designed so that the response of this loop (motor position control) is significantly faster than the response of the outer loop (tip position control) and without any overshoot. It was shown in [1-2] that, in theory, the gains can be made arbitrarily large even if the arm is a non-minimum phase system. Practical limits to these gains are given by the saturation current of the D.C. motor amplifier. Summarizing, we want to achieve two objectives when designing a controller for the motor position:

1. Remove the modeling errors and the nonlinearities introduced by Coulomb friction and changes in the coefficient of the dynamic friction.

2. Make the response of the motor much faster than the response of the tip position control loop (outer loop in Figure 5).

These objectives are accomplished by

1. A feedforward term that compensates for Coulomb friction.

2. A feedforward term that compensates for coupling torque between arm and motors.

3. Closing a high-gain feedback loop which increases the robustness of the system and speeds the motor response.

The fulfillment of the second objective allows us to substitute for the inner loop an equivalent block whose transfer function is approximately equal to '1', i.e. the error in motor position is small and quickly removed. This simplifies the design of the outer loop as will be seen in the next subsection.

3.3 Tip position control loops

In this section, a method to control the tip position of the arm is described. In what follows, we assume that the dynamics of the motor position loops (inner loops) are negligible compared to the dynamics of the arm. If this assumption holds, the arm dynamics may be cancelled using the scheme described in Figure 6. This scheme transforms the arm dynamics into two decoupled double integrators and, therefore, can be considered an extension of the resolved acceleration method [4] to the case of lightweight two-link flexible arms. Once the system has been reduced, two independent P.D. controllers may be designed, one for each coordinate of the tip position. A feedforward term is added to avoid delays when following a trajectory and some integral action is included in the controllers in order to remove small errors due to non exact modelling of the arm kinematics.

The dynamics-cancelling scheme has the following components:

1. A positive feedback loop that uses the motor position calculated from the tip position assuming that there are no deflections in the arm (inverse rigid arm kinematics).

2. The inverse of the jacobian of the rigid arm kinematics. This component transforms the deflections expressed in terms of the tip position (difference in the tip position between the deflected and the undeflected arm for given motor angles) into deflections expressed in terms of motor position (difference in the motor position between the deflected and the undeflected arm for a given tip position).

3. Compliance matrix that relates the forces needed at the tip to move the mass as we want with the deflections needed to achieve this.

4. The inverse dynamics of the rigid arm (model (2)).

Notice that, in this procedure, we are cancelling, block by block, the arm dynamics expressed in Figure 6 (we exclude motor dynamics that have already been cancelled by the inner loop). A scheme equivalent to this one was developed in [2-3] for single-link lightweight flexible arms. Because we use a special configuration that decouples radial from angular motions, components 1 and 2 of the cancelling scheme are very simple: θ_{m1} may be approximately expressed as a linear function of φ and θ_{m2} as a linear function of ρ in component 1; and $\hat{J}$ is a constant diagonal matrix in component 2.

Finally, it should be mentioned that this scheme can be easily extended to lightweight flexible arms of n-degrees of freedom.

4 Experimental results

4.1 Apparatus

We have designed and built an apparatus to enable real-time control experiments with a two-joint, planar arm. As shown in Figure 7, the apparatus comprises of an air table, an arm with a tip mass, two actuators and joint sensors camera for tracking position of tip-mounted, infrared LED and control computer.

The mechanical system was designed to closely approximate the behavior of the ideal system; i.e., the arm is very lightweight, carries an effective point mass at its tip and has minimal friction and backlash. The arm is constructed from music wires, .047 inch and .063 inch in diameter and has a total mass of about .045 lb m. The tip mass is a disk that floats on the air table and has a pivoted connection so that it does not generate torques on the tip of the arm; thus it appears to the arm as a mass concentrated at the tip. Tip mass is adjustable by using different disks, but is typically 0.12 lb m. The tip mass is substantially greater than arm mass and, hence, a lumped-mass model is reasonable. Small ball bearings used at the three passive joints of the arm minimize friction. Tests have shown that the friction on the air table have negligible effect on the behavior of the system. The dimensions of the arm are: l = 9 in., O-A = 3 in., and B-C = 1.5 in. A strut was connected between the middle points of bars A-B and C-O in order to prevent buckling in link A-B and to minimize the deviation from ideal behavior due to unequal bending in the two links.

Joint actuators are DC torque motors. An Inland QT-2404B motor, rated at 36 lb in. peak torque, drives the base link (O-A) directly.

A second motor, Inland model QT-1207D, rated at 1.25 lb in., rides on the base link and generates torque between the base link (O-A) and first link (O-C), through a 3:1 gear reduction. Torques available from the motors are greater than the bending strength of the arm, so torque limits are not a factor in the tip-control servo. Motor response is generally fast compared to the tip response although this is affected by amplifier current limits which are adjusted in the range of .5 to 4 amps. One Inland model EM19-48030-B01 linear current amplifier is used for each motor. Experiments showed that Coulomb friction at the motor joints is considerable, so our method is especially appropriate for the control of this arm.

Three sensors are provided for control: one for each of the two joints and one for the tip. Joint sensors are single-turn potentiometers connected directly to the motor shafts: a 2 in. unit for the larger motor (QT-2404) and a 7/8 in. unit for the smaller. A Hamamatsu tracking camera, model PSD, with infrared passing filter, provides ±5v signals for the x and y positions of an LED attached to the tip. Range of travel within the field of view of the camera is between 7-15 in. on X-axis and about ± 4 in. on Y-axis.

A Sun/Ironics computer system provides for real-time control, program development, and data display and analysis. The system includes a Sun 3/160 workstation and Ironics IV3201 CPU connected via the Sun VME bus and Ironics IV1645-01 A/D and IV1640-01 D/A boards provide analog input and output. The Sun provides a networked Unix environment for program development, interface with the the real-time control hardware, and the storage and display of data. Control programs are written in "C" and compiled to run on the Ironics CPU under the Chimera operating system developed at CMU for real-time control. Chimera provides process scheduling and control primitives that facilitate real-time control programming while emulating many UNIX utilities for programming convenience.

4.2 Identification

The dynamics of the arm was divided (for modelling and control purposes) into two submodels: motors submodel and mechanical structure submodel. These submodels are coupled by the torques at the two motors. It has been shown that this way of modelling flexible arms has some advantages over other methods when dealing with arms with large Coulomb friction in the joints [1-3]. In our identification procedure, we follow this approach and identify both submodels separately.

4.2.1 Mechanical Structure

The experimental method described in Subsection 2.3 is used to identify the dynamics of the mechanical structure. The two motors are immobilized, the arm is deflected by applying an arbitrary force to the tip and then the tip is released. The oscillation produced at the tip has two orthogonal components of different frequencies as was stated in Section 2. They were measured experimentally and agreed with the theoretical analysis (5) - (8). In order to find the two vibrational modes and their directions, we used the following technique:

1. Record the x-y motion of the tip.
2. Calculate the Fourier transform of these two signals $x(t)$ and $y(t)$.
3. The spectral analysis shows that $X(\omega)$ presents two peaks x_1 and x_2 at frequencies ω_1 and ω_2; and $Y(\omega)$ has other two peaks y_1 and y_2 at the same frequencies ω_1 and ω_2 as $X(\omega)$. ω_1 and ω_2 are the frequencies of the two vibrational modes. The directions of the axes of oscillation are calculated from the expression:

$$\psi_i = \arctan(\frac{y_i}{x_i}) \quad i = 1, 2. \tag{12}$$

This procedure is repeated for different arm configurations (different ρ). Fourier transforms are obtained using the FFT routine of the $MATRIX_x$ (a CAD package for analysis and simulation of control systems). Experimental results for our arm are given in Table 1.

ρ (in.)	ω_1 (Hz.)	ψ_1 (deg)	ω_2 (Hz.)	ψ_2 (deg)	k_b (in. lb)	k_c (in. lb)
10.1	0.6514	13.7781	2.1983	106.1437	11.57	6.14
10.55	0.6839	14.3237	2.1332	102.3821	12.3	6.54
11.0	0.6839	15.3966	2.0844	104.9338	11.6	6.58
11.6	0.7328	17.2057	1.9866	103.7644	12.9	6.77
12.2	0.7491	19.0925	1.9215	104.1487	12.5	6.82
12.6	0.7653	20.9127	1.9052	111.4644	12.5	6.87
13.0	0.7816	22.6677	1.90	112.6137	12.3	6.99
13.6	0.7979	26.173	1.9215	116.3932	11.9	7.0
14.0	0.7979	28.5903	1.8889	119.2472	11.3	6.75

Table I. Experimental vibrational modes.

The stiffnesses of the single links k_b and k_c are calculated using the following procedure:

1. Calculate the compliances c_u and c_v in the principal coordinate axes using the expression

$$c_u = \frac{1}{m\omega_1^2}, \quad c_v = \frac{1}{m\omega_2^2}.$$

2. Calculate matrix C, from c_u and c_v. This is done by performing a matrix transformation that corresponds to rotating an angle ψ_1 about the main axes.
3. Calculate k_b and k_c from expressions (10)-(12).

These experimental results show that the values of k_b and k_c are quite consistent, hence their average values, k_b = 12.1 and k_c = 6.7, will be used in the control. Notice that both modes are approximately orthogonals: $\psi_2 = \psi_1 + 90$.

Finally, in order to complete the verification of our theoretical model, we took out the strut between bars A-B and C-O (to simplify the model and the verification) and repeated the experiment for one configuration. The following results were obtained

ρ (in.)	ω_1 (Hz.)	ψ_1 (deg)	ω_2 (Hz.)	ψ_2 (deg)	k_b (in. lb)	k_c (in. lb)
10.55	0.6188	11.5842	2.003	100.6535	9.09	6.39

The theoretical individual stiffnesses were calculated for this case, using our massless flexible arm model, and they were: 9.02 in. lb and 6.63 in. lb, which agreed with the result of this last experiment. All these results confirm the assumption of arm with massless links and joints, with all its mass concentrated at the tip.

4.2.2 Motors Parameters

In order to identify the motor submodel, the mechanical structure (links) was taken out from the motors. As a result, the coupling torque between motors and arm was zero (Ct_i in expression (10)) and the motors could run freely. In what follows, the parameters of the second motor (which has some reduction) are not given in motor terms but in joint terms.

First, we identified the Coulomb friction CF_i by measuring the current at which the motors start to move and their values are: 0.12 $amps$. for the first motor and 0.16 $amps$. for the second. Once the values of the Coulomb friction are obtained, we are able to approximately compensate for the Coulomb friction by adding a term to the current with the estimated absolute value and the sign of the motor velocity as was described in Subsection 3.2.

After compensating for the Coulomb friction, the remaining dynamics of the motors are linear and can be identified by any of the standard techniques. The model is now given by

$$\frac{\theta_{mi}(s)}{\hat{i}_i(s)} = \frac{\frac{K_i}{J_i}}{s(s + \frac{V_i}{J_i})}, \quad i = 1, 2. \tag{13}$$

The parameters that remain to be identified are the motor inertia

J_i and the dynamic frictions V_i. The electromechanical constant of the motors K_i are obtained from the catalog. J_i and V_i are estimated from the frequency response of the system.

4.3 Control

4.3.1 Motor control loop

After compensating for the coupling torque and the Coulomb friction, controllers for the motor position were designed so as to make the response of the motors as fast as possible, but without having any overshoot. Limits in the velocity of response were given by the amplifier current limits, which were 4 *amps.* for the first motor and 2 *amps.* for the second. A sampling time of 3 *msec.* was used for the inner loop.

To test the motor control, the tip was kept in a fixed position (12 *in.* or 0 *mrad* in the polar coordinates) and steplike position commands were generated for the motors. The commanded positions for the motors were such that they would have placed the tip in positions between 10.82 *in.* (-50 *mrad*) and 13.18 *inch.* (50 *mrad*) if the tip had been free. Because the tip was fixed at an intermediate position, the arm experienced substantial bending when the motors tried to follow these trajectories and the coupling torques Ct_i were significant. Figure 8 shows the motor responses obtained in this experiment using the control scheme of Subsection 3.2. The responses have nearly zero steady-state error which shows the effectiveness of the coupling torque and Coulomb friction compensation. The settling time is about 80 *msec* in both motors. This means that the time constants of the motor control loops are about 20 *msec.* These dynamics are significantly faster than the dynamics of the mechanical structure (modes of vibration), confirming the assumption that the inner loop dynamics are negligible.

4.3.2 Tip control loop

The scheme of Figure 6 is used here to control the tip position. The motions are directly commanded in polar coordinates so the first block of this figure that transforms the position from cartesian to polar coordinates is not needed. Second order parabolic profiles are used as reference trajectories, so the reference ρ_r describes a parabola and so does γ_r. The sampling time for the tip position control loop is also 3 *msec*, same as the motor loop.

Experiments to control the tip position were carried out using the complete scheme of Figure 6. The arm was moved from the point 10.82 *inch.* (-100 *mrad*) to the point 13.18 *in.* (100 *mrad*) and vice versa at high speed (to go from one position to the other in 0.4 *sec*). Responses are shown in Figures 9 and 10.

5 Conclusions

Lightweight arms have the advantages that they are easy to move and are more efficient than the heavier arms because very little energy is wasted in moving the arm structure. In turn, these arms usually exhibit some flexibility phenomena that cause nearly undamped oscillations to appear in the mechanical structure during the motion.

A two-degree-of-freedom, planar, very lightweight flexible arm was designed, built and controlled in our laboratory. A simple dynamic model was developed for this arm that is based on two submodels: one that describes the motors, and the other describes the mechanical structure. The two submodels are coupled through the torques that the link generates on the motors. A control scheme that is robust to changes in the dynamic friction of the motor and that removes the effects of the Coulomb friction is used to control the tip position of the arm. This control scheme is based on very simple concepts and each term of the controller is designed to perform a specific function: terms that cancel Coulomb friction, terms that decouple the motors from the arm, inner loop control scheme to make the motor response fast, cancelling terms for the mechanical structure dynamics, feedforward term for the tip response, etc. The experimental results show that the performance of the control scheme is quite good.

The control scheme is based on the assumption that motor dynamics are much faster than mechanical structure dynamics. This assumption must be satisfied before closing the tip position loop. The decoupling between radial and angular motions achieved by the four-bar linkage simplifies kinematic considerations, but is not a necessary condition of this control method. Finally, this method may be easily extended to lightweight flexible arms with any number of degrees-of-freedom.

References

1. Rattan, K.S., Feliu, V., and Brown, H.B., "A Robust Control Scheme for Flexible Arms with Friction in the Joints," *1988 NASA - Air Force Workshop on Space, Operation, Automation and Robotics.* Dayton, OH., July, 1988.

2. Feliu, V., Rattan, K.S and Brown H.B., "New Approach to Control Single-Link Flexible Arms. Part II: Control of the Tip Position in the Presence of Joint Friction," *CMU-RI-TR-89-14, Technical Report. Robotics Institute, Carnegie Mellon University.* July 1989.

3. Feliu, V., Rattan K.S. and Brown H.B., "Control of a Single-Link Flexible Manipulator in the Presence of Joint Friction and Load Changes," *1989 IEEE International Conference on Robotics and Automation,* Scotsdale, May 1989.

4. Craig, J.J., *Introduction to Robotics. Mechanics & Control,* Addison-Wesley Publishing Company, 1986.

5. Thomson, W.T., *Vibration Theory and Applications,* Prentice-Hall, 1965.

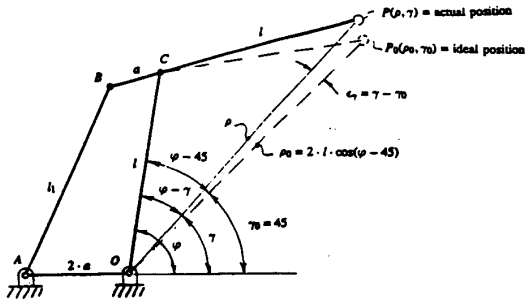

Figure 1: Arm geometry allowing motion only in the second degree-of-freedom.

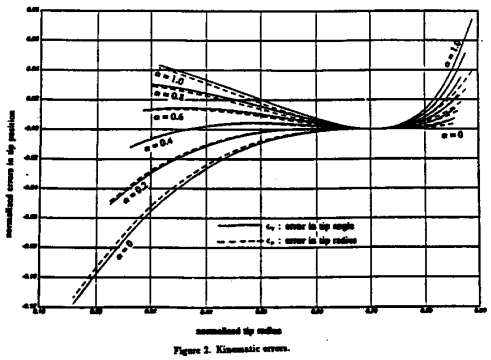

Figure 2. Kinematic errors.

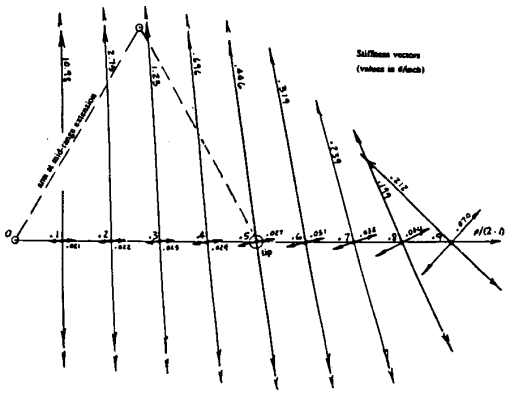

Figure 3. Stiffness plot.

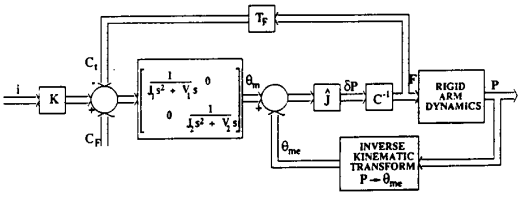

Figure 4. Dynamic model of a lightweight flexible arm.

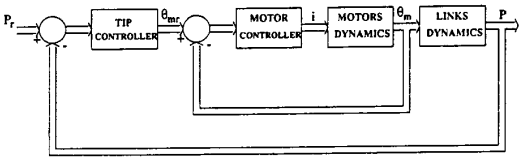

Figure 5. Control scheme that is insensitive to friction.

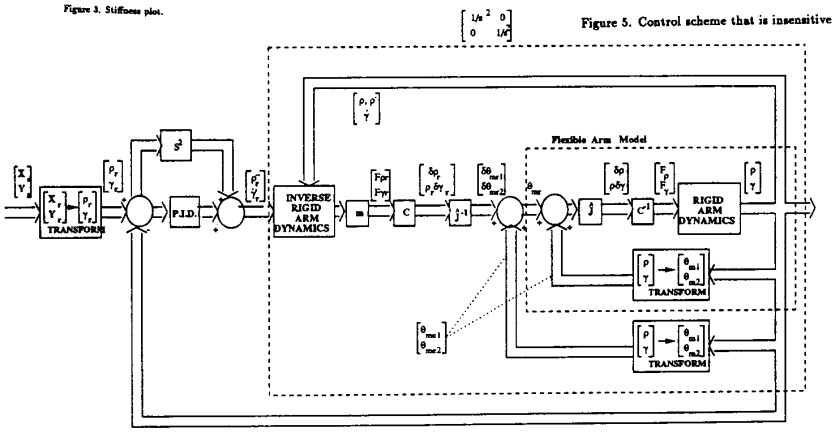

Figure 6: Tip position control scheme as implemented.

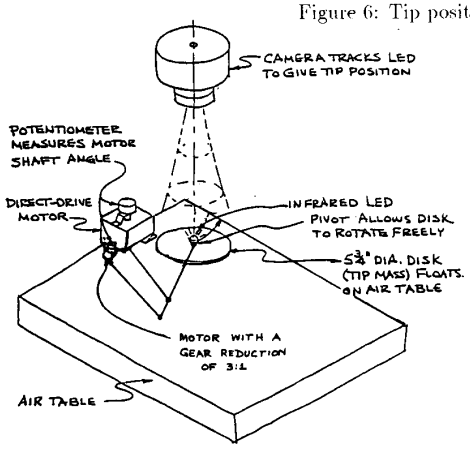

Figure 7. Experimental setup.

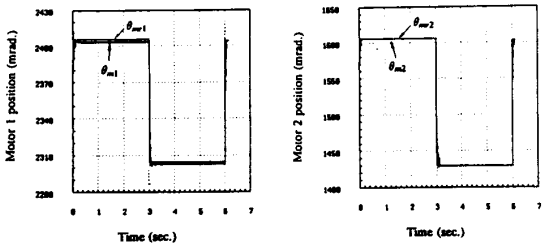

Figure 8. Responses of the inner loop with complete controller.

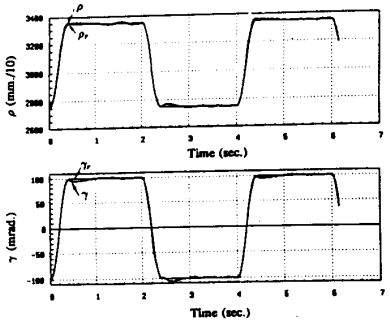

Figure 9. Tip response in polar coordinates.

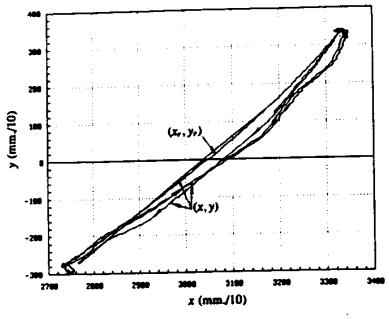

Figure 10. Tip Response in cartesian coordinates.